An experimentally validated model for anodic H_2O_2 production in alkaline water electrolysis and its implications for scaled-up operation

Phadke, Sohan A.; de Jong, Wiebren; Haverkort, J. W.

DOI
10.1016/j.electacta.2024.144258

Publication date
2024

Document Version
Final published version

Published in
Electrochimica Acta

Electrochimica Acta 491 (2024) 144258

Contents lists available at ScienceDirect

Electrochimica Acta

journal homepage: www.journals.elsevier.com/electrochimica-acta

An experimentally validated model for anodic H_2O_2 production in alkaline water electrolysis and its implications for scaled-up operation

Sohan A. Phadke *, Wiebren de Jong, J.W. Haverkort

Process & Energy, Mechanical Engineering, Delft University of Technology, Leeghwaterstraat 39, Delft, 2628CB, Zuid-Holland, Netherlands

ARTICLE INFO

Keywords:
Alkaline water electrolysis
Anodic hydrogen peroxide
Electrochemical reactor model
Hydrogen
Mole balance

ABSTRACT

The anodic co-production of hydrogen peroxide (H_2O_2) during alkaline water electrolysis has gained interest as a sustainable alternative for anthraquinone oxidation. However, electrochemical H_2O_2 production is often studied with idealized laboratory setups to determine the H_2O_2 formation kinetics. In this work, we perform the reaction with industrially relevant operating principles using a flow cell with separately recirculating anolyte and catholyte. We then fit the data to an analytical model that we derive based on mole balances that accounts for anodic generation, anodic oxidation, and bulk disproportionation of H_2O_2, as well as electrolyte volumes and electrode surface area. We performed experiments at 100, 200, and 300 mA cm^{-2} to derive values for the reaction system. At 200 mA cm^{-2}, we found a generation rate of 0.037 mmol min^{-1} cm^{-2} ($FE_{H_2O_2}$ = 59%) and an anodic decomposition rate constant of 0.304 cm min^{-1}, with a bulk disproportionation rate constant of 1.85 × 10^{-3} min^{-1}. We successfully applied our model to two sources in literature to derive values for their systems as well. In all cases, the contribution of anodic oxidation of H_2O_2 was found to be the larger loss mechanism in comparison to bulk disproportionation. Using the analytical model, we show that decreasing the reservoir volume is a simple way to increase the H_2O_2 concentration over time. Further refinement of the model can be achieved through the use of mass transfer relationships based on electrolyzer geometries to describe the anodic oxidation of H_2O_2 in the mole balance equations.

1. Introduction

The use of electrochemistry, when powered by renewable energy resources, offers a promising pathway for the sustainable production of chemicals. One of these chemicals that requires a more sustainable pathway is hydrogen peroxide (H_2O_2), which is used as a green oxidant in industries such as paper milling and textile bleaching [1,2]. However, it is currently produced by the anthraquinone oxidation process, which has a large energy demand of 17.6 kWh kg^{-1} due to high solvent use and separation requirements [3–5]. A more sustainable route would be via alkaline water electrolysis. During alkaline water electrolysis, we typically produce hydrogen gas (H_2) at the cathode and oxygen gas (O_2) at the anode [6]. While research into the cathodic co-production of H_2O_2 via oxygen reduction reaction is more commonly investigated, cathodically produced H_2O_2 has some notable drawbacks. One drawback is that in order to effectively deliver oxygen to the cathode, a more complex gas-diffusion electron must be used, which can lead to mass transfer limitations. The other issue is that in cathodic H_2O_2 production, the valuable H_2 product is replaced, and the anode still produces low-value O_2 [7]. A more attractive alternative is to instead electrochemically produce H_2O_2 at the anode by carefully selecting the anode material and electrolyte [8]. This form of paired electrolysis makes use of both the cathode, by producing a valuable, carbon-free energy carrier in H_2, and of the anode, by producing a high-value commodity chemical in H_2O_2 alongside O_2.

The main difficulty of anodic H_2O_2 production is that the potential required to produce H_2O_2 is higher than that required to produce O_2. The thermodynamic half cell potential to produce H_2O_2 under alkaline conditions as per Eq. (1) is 1.76 V versus the Reversible Hydrogen Electrode (RHE). Because the thermodynamic half cell potential to produce O_2 is only 1.23 V versus RHE as per Eq. (2), the generation of H_2O_2 at the anode is always in competition with the formation of O_2. While different anode materials may display different selectivities towards H_2O_2 generation over O_2 evolution, there is still no reported material with 100% Faradaic efficiency to H_2O_2.

Much of the research into anodic H_2O_2 production focuses on finding more selective anode materials or on elucidating the reaction mechanism [9–13]. In either case, experiments are typically performed in a one-compartment cell or in a separated H-cell configuration to study the fundamental anode performance over time [14–16]. Experiments are also often performed with refreshed anolyte, or single-pass

* Corresponding author.
E-mail address: s.a.phadke@tudelft.nl (S.A. Phadke).

https://doi.org/10.1016/j.electacta.2024.144258
Received 30 November 2023; Received in revised form 16 March 2024; Accepted 8 April 2024
Available online 9 April 2024

anolyte in the case of flow cells, to avoid the effect of H_2O_2 loss mechanisms [17,18]. A cation exchange membrane such as Nafion 117 is also frequently used, presumably to prevent H_2O_2 crossover to the catholyte. However, this would be inadvisable for an alkaline electrolyzer system as it inhibits the transport of hydroxide (OH^-) anions, which allow the reaction to proceed. In order to scale up a system for industrial electrochemical H_2O_2 production, we must examine how the system behaves with more relevant industrial operating conditions, which include separately recirculating electrolyte flows, a porous separator material, and constant pH and temperature throughout the reaction.

For example, operating a flow cell with single-pass anolyte using high flow rates yields an anolyte product stream with very low H_2O_2 concentration. This low concentration results in a more difficult downstream separation to extract the product. One could feed anolyte at lower flow rates to achieve a higher concentration, but the total H_2O_2 production rate would then be lower. Such lower flow rates come with the drawback of the unavoidable loss mechanisms, namely the anodic oxidation of H_2O_2 as per Eq. (3) at 0.67 V versus RHE, and the disproportionation of H_2O_2 in bulk electrolyte as per Eq. (4). One solution would be recirculating the anolyte at high flow rates for some time before the separation stage, thus increasing H_2O_2 concentration over time, easing downstream separation, and lowering cost. However, recirculating anolyte comes with the same unavoidable loss mechanisms. As H_2O_2-charged anolyte recirculates past the anode, the chance for anodic oxidation of the H_2O_2 increases. Additionally, the increased time for recirculation increases the time for bulk disproportionation to occur in the anolyte reservoir, further decreasing the achieved H_2O_2 concentration. Therefore, we must study how the network of reactions behaves in the relevant case. This network of reactions is shown schematically in Fig. 1.

$$2\,OH^- \rightarrow H_2O_2 + 2\,e^- \qquad E^\circ = 1.76\ \text{V versus RHE} \qquad (1)$$

$$4\,OH^- \rightarrow 2\,H_2O + O_2 + 4\,e^- \qquad E^\circ = 1.23\ \text{V versus RHE} \qquad (2)$$

$$H_2O_2 + 2\,OH^- \rightarrow 2\,H_2O + O_2 + 2\,e^- \qquad E^\circ = 0.67\ \text{V versus RHE} \qquad (3)$$

$$2\,H_2O_2 \rightarrow 2\,H_2O + O_2 \qquad (4)$$

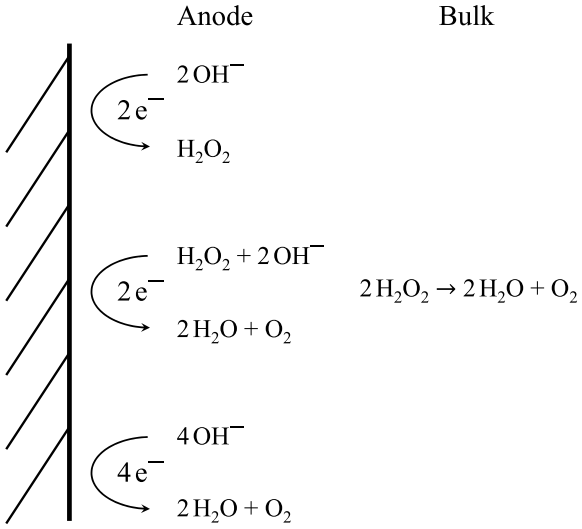

Fig. 1. A simplified schematic of the reactions detailed in Eqs. (1)–(4) occurring in the anode chamber of the electrolyzer, with the anode wall on the left.

In this work, we study an industrially relevant electrolyzer system that separately recirculates anolyte and catholyte, and includes the standard porous separator material used in alkaline water electrolysis, Zirfon Perl UTP 500. We formulate a system of transient mole balance equations for the process and perform experiments to derive individual terms of the mole balance equations. The terms we derive experimentally are the generation rate of H_2O_2 and the rate constant of bulk disproportionation of H_2O_2 in the electrolyte. We then fit our experimental data to the analytical solution of the mole balance equations, which provides the rate constant for the oxidation of H_2O_2 at the anode. We repeat this analysis using data from two references in literature that perform the reaction in a similar manner. Lastly, we simulate a change in design parameters to inform our recommendations on reactor and system design.

Table 1
List of symbols used in this work.

Symbol	Parameter	Units
V_E	Volume of anolyte in anode chamber	L
V_R	Volume of anolyte in reservoir	L
V_A	Total anolyte volume	L
c_{out}	H_2O_2 concentration out of electrolyzer	mM
c_{in}	H_2O_2 concentration into electrolyzer	mM
t	Time	min
$\dot{Q}$	Electrolyte flow rate	L min^{-1}
S	H_2O_2 generation rate	mmol min^{-1} cm^{-2}
k_a	H_2O_2 anodic decomposition rate constant	cm min^{-1}
k_b	H_2O_2 bulk disproportionation rate constant	min^{-1}
k_c	H_2O_2 crossover rate constant	cm min^{-1}
A	Electrode surface area (geometric)	cm^2
A_{sep}	Separator surface area (geometric)	cm^2
ξ	Extent of reaction	–
j	Current density	mA cm^{-2}
$FE_{H_2O_2}$	Faradaic efficiency to H_2O_2	%
$\mathcal{D}$	Effective diffusion coefficient	cm^2 s^{-1}
L_{sep}	Separator thickness	cm

2. Analytical model

2.1. List of symbols

Table 1 lists the variables used in this work and their accompanying units.

2.2. Mole balance equations

We follow the analysis method outlined by Pickett involving two separate mole balances, one over the electrolyzer, and the other over the electrolyte reservoir [19]. In our analysis, we interchangeably use the terms "electrolyzer" and "electrolyzer volume" to denote the anode chamber and the volume of the anode chamber, because they are the system under investigation. A simplified diagram of the system is shown in Fig. 2. The mole balance over the electrolyzer is written in Eq. (5),

$$V_E \frac{dc_{out}}{dt} = \dot{Q}c_{in} - \dot{Q}c_{out} + SA - k_a A c_{out} - k_b V_E c_{out} \qquad (5)$$

where V_E/L is the volume of the anode chamber, $c_{out}(t)$/mM is the concentration of H_2O_2 out of the electrolyzer, t/min is time, $\dot{Q}$/L min^{-1} is the volumetric flow rate of electrolyte, $c_{in}(t)$/mM is the concentration of H_2O_2 going into the electrolyzer, S/mmol min^{-1} cm^{-2} is the constant anodic generation rate of H_2O_2, A/cm^2 is the geometric anode surface area, k_a/cm min^{-1} is the rate constant for anodic oxidation of H_2O_2 as per Eq. (3), and k_b/min^{-1} is the rate constant for bulk disproportionation as per Eq. (4). Note that these units require the anodic oxidation term, k_aA, to be multiplied by a conversion factor of 0.001 L cm^{-3}, which carries throughout.

A similar mole balance is expressed in Eq. (6) for the change in concentration across the electrolyte reservoir,

$$V_R \frac{dc_{in}}{dt} = \dot{Q}c_{out} - \dot{Q}c_{in} - k_b V_R c_{in} \qquad (6)$$

where V_R/L is the reservoir volume. The total anolyte volume, V_A/L, is equal to $V_E + V_R$. This definition treats the small volume of electrolyte in the tubing between electrolyzer and reservoir as belonging to the reservoir, and is addressed in Section 3.1. The terms involving S and k_a appear only in the electrolyzer mole balance, while the term involving k_b appears in both balances, as bulk disproportionation can occur everywhere.

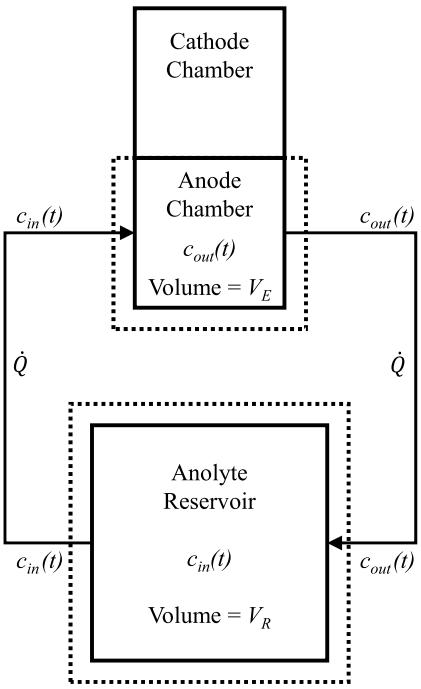

Fig. 2. A simplified diagram of the overall system. The dashed boxes indicate the boundaries of the mole balance equations.

2.3. Assumptions

We assume a perfectly mixed anode chamber due to bubble mixing and flow such that the outlet concentration of the electrolyzer, $c_{out}(t)$, is the concentration everywhere in the anode chamber, including the anode surface. This assumption is acceptable for systems with low single-pass conversion rates, which for our system was between 0.9% and 3.0%, validating the assumption. We similarly assume a perfectly mixed anolyte reservoir, which we achieve experimentally via magnetic stirring. We also assume that V_A, V_E, V_R, and $\dot{Q}$ are constant.

In Eq. (5), we express the anodic oxidation of H_2O_2 as a surface reaction described by a first order rate equation using a homogeneous H_2O_2 concentration in the electrolyzer. This is a simplifying assumption for a surface concentration that would actually involve a mass transfer term, [6] but it allows us to more easily express the reaction term without involving more complex mass transfer relationships for various electrolyzer geometries. Incidentally, a mass transfer limited reaction would also be expected to be a first order reaction, so this generalized form may cover more than one possible situation.

We assume that only the reactions in Eqs. (1)–(3) take place at the anode. We further assume that S is constant, although in reality there will be a ratio of how much current goes towards H_2O_2 generation versus H_2O_2 oxidation, O_2 evolution, or any other side reactions at the anode. Finally, we assume that there is no loss of H_2O_2 due to crossover into the catholyte. This was observed experimentally and further examined in Section 4.4.

2.4. Solutions

Eq. (6) can be rearranged to solve for $c_{out}(t)$ as a function of $c_{in}(t)$, and then differentiated to find an expression for $dc_{out}(t)/dt$ as a function of $c_{in}(t)$. These expressions can be used to eliminate c_{out} from Eq. (5), leading to the second order, non-homogeneous differential equation in Eq. (7),

$$\frac{d^2c}{dt^2} + \left(\frac{\dot{Q}}{V_E} + \frac{\dot{Q}}{V_R} + \frac{k_aA}{V_E} + 2k_b\right)\frac{dc}{dt} + \left(\dot{Q}\left(\frac{k_aA}{V_EV_R} + \frac{k_b}{V_R} + \frac{k_b}{V_E}\right) + \frac{k_aAk_b}{V_E} + k_b^2\right)c = \frac{SA\dot{Q}}{V_EV_R} \tag{7}$$

where we have dropped the subscript of $c_{in}(t)$ and examine simply $c(t)$/mM, the concentration of H_2O_2 in the anolyte reservoir over time.

We make a final simplification of Eq. (7) for the case that the flow rate, $\dot{Q}$, is very large. The full solution to Eq. (7) and the justification of the high flow rate assumption are shown in Appendices A and B. In the case of large $\dot{Q}$, the $\dot{Q}$ term cancels out and we obtain the first order differential equation in Eq. (8).

$$\frac{dc}{dt} = \frac{SA}{V_E + V_R} - \frac{k_aA}{V_E + V_R}c - k_bc \tag{8}$$

Using the initial condition that $c(t) = 0$ at $t = 0$, we reach the final result in Eq. (9).

$$c = \frac{SA}{k_aA + k_b(V_E + V_R)}\left(1 - \exp\left(-\left(\frac{k_aA}{V_E + V_R} + k_b\right)t\right)\right) \tag{9}$$

As t approaches ∞, we find the expected steady state concentration in Eq. (10), which takes the form of the H_2O_2 generation term over a weighted sum of the H_2O_2 decomposition terms.

$$c_{\text{Steady State}} = \frac{SA}{k_aA + k_b(V_E + V_R)} \tag{10}$$

We can also define an extent of reaction, $0 \le \xi < 1$, such that $\xi c(t)$ is the fraction of the steady state concentration reached in the anolyte. Using this definition and solving for t_ξ, the time it takes to reach ξ fraction of the steady state concentration, we arrive at Eq. (11).

$$t_\xi = \frac{-\ln(1-\xi)}{\left(\frac{k_aA}{V_E+V_R} + k_b\right)} \tag{11}$$

3. Methods

3.1. Materials

Experiments were performed using a flow cell constructed of laser-cut PMMA sheets with silicone and EPDM gaskets layered in between, compressed together with bolts. Titanium plates were used as current collectors, and the electrodes were kept at a distance of 0.7 cm to the separator. The anode and cathode chamber dimensions were 3 cm wide by 4 cm tall by 0.7 cm deep (V_E = 0.0084 L). The cathode was nickel fiber felt (12 cm^2, geometric) from Hebei Aegis Metal Materials Co., Ltd, 0.4 mm thickness, with 40 μm fiber diameter and 60% porosity. The anode was boron-doped diamond (2.5 cm × 4 cm = 10 cm^2, geometric) from NeoCoat on a niobium substrate, with 5 μm thick, p-doped, 2500 ppm boron doping, polycrystalline coating. The separator used was the porous diaphragm, Zirfon Perl UTP 500 (Agfa) with a thickness of 500 μm. The electrolyte used was 1 M Na_2CO_3 (Merck-Sigma, ACS Reagent, ≥ 99.5%, powder or granules) plus 11 g L^{-1} (approximately 90 mM) Na_2SiO_3 (Merck-Sigma, SKU 307815). Flow was maintained at 0.1 L min^{-1} using a Longer BT100-3J peristaltic pump with DG15-24 two-channel pump head, with the anolyte and catholyte recirculated separately. The tubing for anolyte held a volume of 8.04 cm^3, which was negligible compared to the anolyte volume of V_A = 0.4 L. The anolyte reservoir was magnetically stirred to ensure good mixing.

Because S, k_a, and k_b are expected to vary based on temperature, pH, electrolyte composition, presence of a stabilizer, etc., these parameters were kept constant across all experiments. The anolyte pH was maintained between 13.25 and 13.10, just above the base electrolyte pH of 13.10, by manual monitoring and addition of aliquots of 5 M NaOH (Merck-Sigma, ACS Reagent, ≥ 97.0%) solution. The high NaOH concentration served to lower the amount of anolyte volume change upon NaOH addition. The overall combination of reaction, sampling, NaOH addition, and any possible liquid flux through the porous separator resulted in overall volume changes of < 10% over 7 h across all experiments. The temperature was controlled to be just

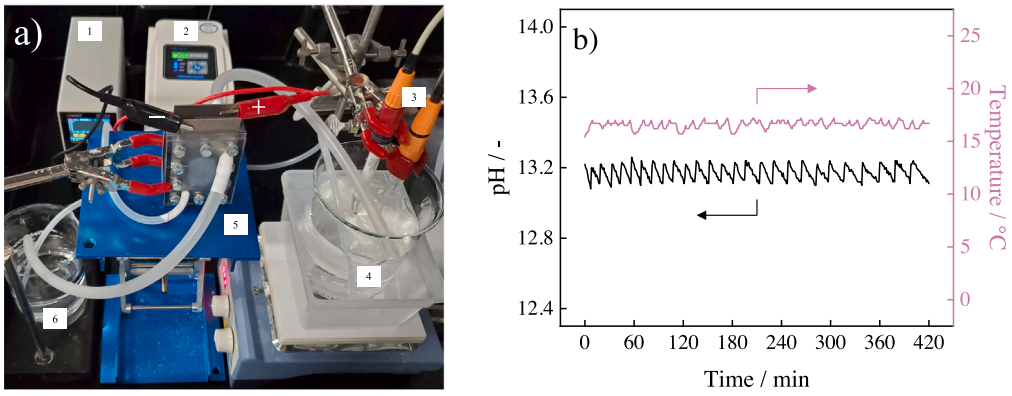

Fig. 3. (a) Photo of the experimental setup with (1) power supply (2) two-channel peristaltic pump (3) pH and temperature sensors (4) Anolyte reservoir with magnetic stirring and external container for cold water bath (5) electrochemical flow cell with cathode compartment near and anode compartment away (6) catholyte reservoir. (b) Plot of the maintained pH and temperature of the anolyte reservoir for a typical experiment with recirculating flows. The vertical spikes in pH were the moments of NaOH solution addition, and are required less frequently as the pH of the catholyte slowly increases during the experiment.

under room temperature, at approximately 16 ± 1 °C, by immersing the anolyte reservoir in a cold water bath. The anolyte pH and temperature were measured using a Prominent PHEP-H 314 SE sensor and a Prominent Pt 100-SE sensor, respectively. Catholyte was recirculated for all experiments, with no maintenance of pH or temperature. Fixed current (galvanostatic operation) was supplied at 1.0, 2.0, or 3.0 A in two-electrode operation using an OWON SPE6103 power supply. Fig. 3(a) shows a photo of the experimental setup and Fig. 3(b) shows the typical curves for pH and temperature in the anolyte reservoir over time during an experiment with recirculating flows.

3.2. H_2O_2 quantification

The H_2O_2 concentration was quantified using the potassium permanganate ($KMnO_4$) titration method as outlined by Gill et al. [20]. In short, the method comprises of taking a sample of electrolyte (typically 2.5 mL) and immediately acidifying with equal volume of a 1:5 dilution of H_2SO_4 (Merck-Sigma, 95%–98%, ACS Reagent) in milli-Q water (Merck-Millipore, resistivity = 18.2 MΩ cm). Electrolyte samples from both anolyte and catholyte were taken from the reservoirs at regular intervals. For single-pass experiments, electrolyte was sampled directly from the reactor outflow. The titrant used was a 2 mM solution of $KMnO_4$, diluted ten-fold from stock solution (Merck-Sigma, 0.02 M, standardized against oxalate, Titripur). To start, three drops of 2 mM $KMnO_4$ solution were added to the magnetically stirred, acidified sample until the pink color disappeared (starting the reaction). These three drops defined the limit of quantification for a 2.5 mL sample to be 0.3 mM. The titrant was further added drop-wise until a light-pink color remained in the sample, indicating the titration endpoint.

3.3. Determination of S

The majority of literature shows that for fresh electrolyte passed across the anode, the generation of H_2O_2 tends to be constant over time for a fixed operating potential [17,18]. This observation could also be reasoned for an electrode that is very stable over time, such as boron-doped diamond. So for a corresponding fixed current density, this formation rate can be expressed as,

$$S = \frac{\dot{Q} c_{SinglePass}}{A} = \frac{j}{n\mathcal{F}} \mathrm{FE}_{H_2O_2} \tag{12}$$

where $c_{SinglePass}$ is the H_2O_2 concentration achieved in electrolyte flown in single-pass over the anode, j is the current density, n=2 is the ratio of moles of electrons to moles of H_2O_2, $\mathcal{F}$ is Faraday's constant, and $\mathrm{FE}_{H_2O_2}$ is the Faradaic efficiency towards H_2O_2. The generation rate, S, for a single current density can be experimentally quantified by flowing electrolyte in single-pass at a high flow rate and measuring the outlet H_2O_2 concentration immediately. The high flow rate and quick measurement ensure that the residence time for anodic oxidation and the time for bulk disproportionation are low enough to be negligible. Fig. 4 shows the schematic of the flow setups of the experiments. The first expression in Eq. (12) can be used to find a value for S from the experiment, while the second can be used to calculate the Faradaic efficiency.

3.4. Determination of k_b

The experimental determination of the rate constant for bulk disproportionation, k_b, required first running the electrolyzer with recirculating flow in order to charge the anolyte with H_2O_2. After two hours of operation with pH and temperature maintained, the electrolyzer

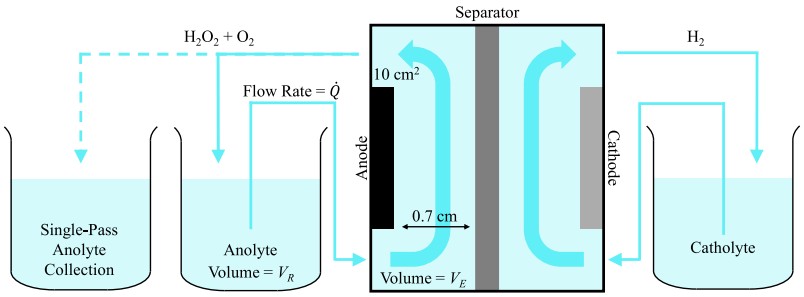

Fig. 4. Diagram of the different flow configurations (not to scale). The solid arrow leaving the anode chamber and returning to the anolyte reservoir represents recirculating flow, while the dashed arrow leaving the anode chamber towards a separate collection vessel represents single-pass flow. For experiments using recirculating flow, anolyte is sampled from the reservoir. For experiments using single-pass flow, anolyte is sampled directly from the outlet of the anode chamber, not the collection vessel.

contents were drained into the reservoirs, and samples of anolyte were periodically taken for H_2O_2 quantification. This procedure was performed for three different current densities in order to compare concentration curves with different initial concentration values.

3.5. Numerical fitting of k_a

Because the anodic oxidation of H_2O_2 is an electrochemical reaction, k_a is expected to increase as the cell potential increases. However, due to its lower thermodynamic half cell potential of $E°$ = 0.67 V versus RHE compared to the generation of H_2O_2 at 1.76 V versus RHE, these two reactions are in direct competition. As such, k_a cannot be independently measured. Instead, after experimentally deriving values for S and k_b as described in Sections 3.3 and 3.4, the electrolyzer is run for seven hours with recirculating flow. Samples of electrolyte are taken for H_2O_2 quantification as described in Section 3.2. With the known values of V_E and V_R, the data points of $c(t)$ for a given current density are fitted to Eq. (9) in Python using the 'curvefit' function from the SciPy module. This function runs a non-linear least squares regression to find the best fit. Fitted parameters were given no constraints and only supplied with an initial guess to ease computation.

4. Results and discussion

4.1. H_2O_2 generation

The results of the single-pass flow experiments are shown in Fig. 5(a). Using the average concentrations at each of the three current densities, we use Eq. (12) to calculate S = 0.017, 0.037, and 0.054 mmol min^{-1} cm^{-2} at 100, 200, and 300 mA cm^{-2}, respectively. The calculated Faradaic efficiencies at each of the three current densities were similar, with values of 54%, 59%, and 58% for 100, 200, and 300 mA cm^{-2}, respectively. These constant H_2O_2 generation rates and the calculated Faradaic efficiencies are consistent with the literature report of boron-doped diamond materials by Mavrikis et al. using refreshed electrolyte [17]. At the same current densities in 1 M carbonate/bicarbonate electrolyte, they report H_2O_2 generation rates between 0.016 and 0.076 mmol min^{-1} cm^{-2} and Faradaic efficiencies between 50% and 70% for a set of boron-doped diamond anodes.

4.2. H_2O_2 loss via bulk disproportionation

The results of the experiments for k_b quantification are shown in Fig. 5(b). Each of the curves represent a batch of anolyte that was charged with H_2O_2 for two hours at 100, 200, or 300 mA cm^{-2} with separately recirculating flows. The power supply was then switched off, its contents drained, and the anolyte concentration was measured over time. Literature indicates that the disproportionation of H_2O_2 should be a first order decomposition reaction [21]. Examining the data, we see a constant slope on a semi-log plot for all three data sets, indicating a first order decomposition reaction with an average rate constant of 1.85 × 10^{-3} min^{-1}. This value is consistent with the value for bulk disproportionation found by Li et al. who used an electrolyte of 2 M $KHCO_3$ at room temperature, and Lee et al. who studied H_2O_2 decomposition for a range of electrolytes including Na_2CO_3 with Na_2SiO_3 stabilizer [21,22].

4.3. Full system - Fitting k_a

After deriving S and k_b, we now perform seven hour experiments with separately recirculating electrolyte, a porous Zirfon separator, and with anolyte pH and temperature maintained. Fig. 6 shows the accumulation of H_2O_2 over time in the system, along with the fit of Eq. (9). The fitted values of k_a are 0.136, 0.304, and 0.349 cm min^{-1} at 100, 200, and 300 mA cm^{-2}, respectively. The modified anodic decomposition term as it appears in Eq. (8), $(k_aA)/(V_E + V_R)$, was calculated to be 3.40 × 10^{-3}, 7.59 × 10^{-3}, and 8.73 × 10^{-3} min^{-1}, in order of increasing current density. These values are all greater than k_b = 1.85 × 10^{-3} min^{-1}, indicating that the anodic oxidation of H_2O_2 in the anolyte was the dominant loss mechanism in our system. The fit appears to match the experimental results well, though there is a slight underprediction of the concentration at t < 240 min and a slight overprediction of the steady state concentration at t > 360 min. This likely originates from our definition of the constant generation of H_2O_2. In the case of a competing surface reaction, S would no longer be constant, but be expected to decrease over time as $c(t)$ increased over time, due to the increased rate of anodic oxidation. Nevertheless, the fit is good and displays the expected trend of increasing k_a with increasing current density.

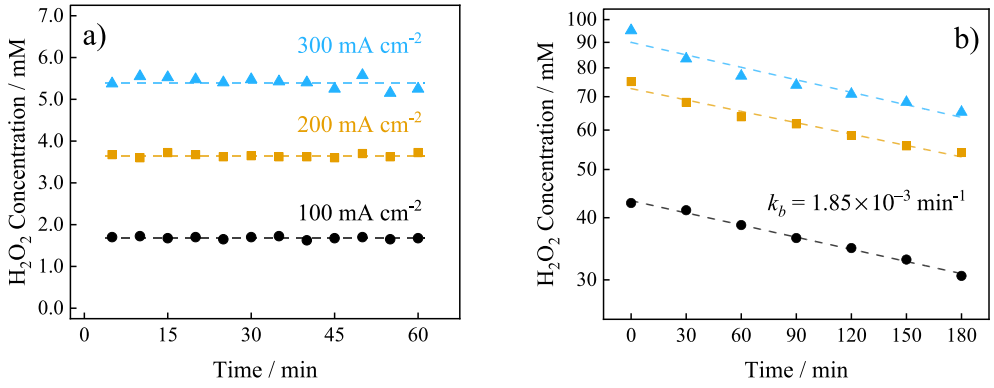

Fig. 5. (a) The constant generation of H_2O_2 under single-pass flow for a given current density. The dashed lines indicate the average measured concentrations over one hour of 1.68, 3.65, and 5.40 mM at 100, 200, and 300 mA cm^{-2}, respectively. These average concentrations are used to calculate S = 0.017, 0.037, and 0.054 mmol min^{-1} cm^{-2}, in order of increasing current density. (b) Comparison in semi-log scale of the homogeneous decomposition of H_2O_2 in anolyte from different starting concentrations without applied current. These starting concentrations were achieved by operating the electrolyzer with recirculating electrolyte flow for two hours at different current densities. Dashed lines are linear regressions of the data sets. These data sets share a constant slope, indicating a first order bulk disproportionation reaction with an average rate constant of k_b = 1.85 × 10^{-3} min^{-1}.

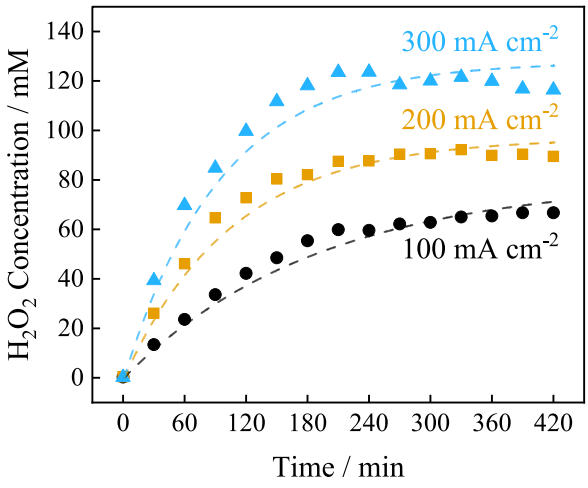

Fig. 6. Seven-hour experiments for the anodic production of H_2O_2 with recirculating anolyte. The dashed lines show Eq. (9) using fitted k_a values of 0.136, 0.304, and 0.349 cm min^{-1} for 100, 200, and 300 mA cm^{-2}, respectively.

4.4. Exclusion of crossover effects

It was observed that the H_2O_2 concentration in the catholyte was always at or below the limit of quantification (0.3 mM as mentioned in Section 3.2). This indicated that either the decomposition of H_2O_2 in the catholyte far outpaced the diffusive flux through the Zirfon separator, or that the diffusive flux itself was negligible. At pH greater than the pKa of H_2O_2 (11.7), the H_2O_2 exists primarily in its deprotonated form as HO_2^-. This anion experiences a force of electric migration towards the anode, which is in the opposite direction of the diffusive flux. We therefore reason, as we operate at pH > 13, that nearly all of the anodically produced H_2O_2 is retained in the anolyte. To confirm this, we modify Eq. (5) to add a term to account for H_2O_2 crossover, $-k_c A_{sep} c_{out}(t)$, where A_{sep} is the separator surface area. The k_c term can be calculated by analogy to Fick's law for diffusion across the separator, assuming a concentration of zero on the cathode side, as per Eq. (13),

$$k_c = \frac{\mathcal{D}}{L_{sep}} \tag{13}$$

where k_c/cm min^{-1} is the rate constant for crossover, $\mathcal{D}$ is the effective diffusion coefficient, and L_{sep} is the thickness of the separator. Using the values of our setup (A_{sep} = 12 cm^2 and L_{sep} = 0.05 cm) and assuming a typical liquid diffusion coefficient at ambient temperature of $\mathcal{D} = 1 \times 10^{-5}$ cm^2 s^{-1}, we find $k_c = 2.0 \times 10^{-4}$ cm min^{-1}. The modified crossover term as it would appear in Eq. (8), $(k_c A_{sep})/(V_E + V_R)$, was calculated to be 3.60×10^{-4} min^{-1}. Comparing this value to the anodic decomposition terms that we found in Section 4.3 (all $\geq 3.40 \times 10^{-3}$ min^{-1}), we see that any effect of crossover is negligible in comparison to the anodic oxidation in the anode chamber. The modified crossover term is also negligible in comparison to the bulk decomposition rate constant of 1.85×10^{-3} min^{-1}.

4.5. Extension to literature data

One of the strengths of the outlined analytical model is that knowledge of the precise details of the system are not required. Neither the specific reaction mechanism for H_2O_2 generation, the particular electrolyte composition, nor the electrolyzer geometry have to be taken into consideration. The only relevant parameters are the physical dimensions (A, V_E, and V_R), the overall generation rate (S), and the rate constants (k_a and k_b). As such, the model remains versatile. We demonstrate this versatility by examining two sources from literature, Pangotra et al. [23] and Li et al. [22], and use their data to calculate rate constants as per their experimental setups.

The setup of Pangotra et al. uses a 10 cm^2 anode and an electrolyte flow rate of 0.1 L min^{-1}, and is very similar to our own. The main difference is that they use Nafion 117 as a separator and keep their anolyte in an ice bath to maintain the temperature. Using their data, we found a k_b value of 5.70×10^{-4} min^{-1} for 2 M K_2CO_3 with 90 mM Na_2SiO_3 electrolyte. This value is about three times lower than for our system, which is consistent with a lowered reaction rate due to lower temperatures. We fitted their data for both S and k_a at the same current densities as we use, and the fit is shown in Fig. 7(a). The fitted curve shows excellent agreement, likely due to the additional free parameter available for fitting, S. Table 2 lists the computed values for all of the experimental data sets analyzed. The values of S from Pangotra et al. are comparable to ours, but the k_a values are much higher, particularly at 300 mA cm^{-2}. This leads to their overall lower steady state concentrations and their observed optimal current density of 200 mA cm^{-2}.

The setup used by Li et al. was not a flow setup but rather a separated batch reactor system. The anolyte was magnetically stirred to ensure mixing. Li et al. operate their system potentiostatically, but observed a relatively constant current at each potential, allowing our analysis to continue. While they do not maintain pH or temperature, they operate at low currents of < 35 mA and observe a very small pH change from 8.31 to 8.68. We therefore assume that the temperature and pH have not changed significantly over the course of the experiment, such that the model can still be applied. The analytical model can be reformulated by simply setting V_R and $\dot{Q}$ equal to zero, which causes Eq. (6) to cancel out entirely. The resulting mole balance across the electrolyzer takes the following form.

$$V_E \frac{dc_{out}}{dt} = SA - k_a A c_{out} - k_b V_E c_{out} \tag{14}$$

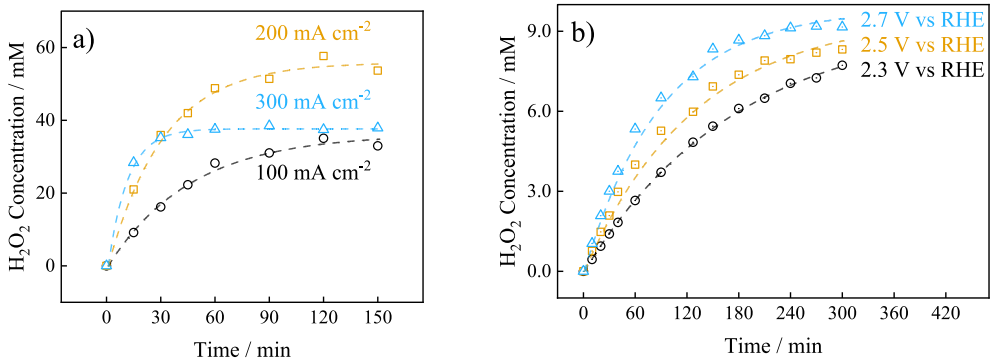

Fig. 7. Fits to data from literature sources, with open symbols to indicate data points not from our work. See Table 2 for a summary of parameter values. (a) Dashed lines showing the fit of Eq. (9) to the data of Pangotra et al. [23]. Both S and k_a were fitted to this data using k_b from their data. (b) Dashed lines showing the fit of Eq. (15) to the data of Li et al. [22]. Only k_a was fitted to this data using S and k_b from their data.

The solution to Eq. (14), replacing c_{out} with c, is shown in Eq. (15),

$$c = \frac{SA}{k_a A + k_b V_E}\left(1 - \exp\left(-\left(\frac{k_a A}{V_E} + k_b\right)t\right)\right) \quad (15)$$

where V_E = 0.06 L is the anolyte volume. Eq. (15) takes the same overall form as Eq. (9), but setting V_R equal to 0. This is a result of all reactions taking place in the same batch reactor, without a separate reservoir. Li et al. [22] arrive at a similar expression to Eqs. (9) and (15) and fit it successfully to their data. However, they combine their k_a and k_b terms into a single parameter and neglect the solution volume and electrode surface area. Our more versatile analytical model based on mole balances successfully accounts for these differences, and the fit of Eq. (15) to their data is shown in Fig. 7(b). Our fit matches well to the experimental data obtained by Li et al. However, the data sets do not continue until a very clear steady state, so we cannot comment on any underprediction or overprediction of the model with respect to time. Li et al. performed a similar experiment to quantify the contribution of bulk disproportionation as we did and found k_b = 1.83 × 10^{-3} min^{-1} [22]. This value is very close to the value for our system, despite using a different electrolyte of 2 M $KHCO_3$. The values of S (calculated using data from Li et al.) are significantly lower than our values due to the lower total current of their experiments with a 0.5 cm^2 anode, but follow the predicted trend of increasing with increasing current density (see Table 2). However, the k_a values (fitted) are quite large, and are comparable to those of Pangotra et al. who operate at much higher current densities. These large anodic decomposition rate constant values may also have led to the lower concentrations seen in the experiments of Li et al. This result highlights the drawback of running such a system in batch reactor, as there is a large opportunity for any produced H_2O_2 to oxidize further. In contrast, a flow cell system has a lower residence time of H_2O_2 in the electrolyzer, thereby lowering the chance for anodic oxidation of H_2O_2.

4.6. Model validation and implications for scaled-up operation

The scaled-up electrochemical process to produce H_2O_2 with high flow rates faces the obstacle of low single-pass conversion. A low H_2O_2 concentration makes later separation and purification more difficult, and low flow rates result in overall low product yield, thus necessitating anolyte recirculation to charge it with higher concentrations of H_2O_2. The objective of the process design should then be to maximize H_2O_2 concentration in the anolyte stream in the minimum required time. While S, k_a, and k_b are dependent on the electrode–electrolyte system chosen, A, V_E, V_R, and $\dot{Q}$ can all be easily changed as desired to fit the requirements of a separation system or target production rate.

To validate our model's ability to predict the change in $c(t)$ with varying V_E or V_R, we perform experiments at 200 mA cm^{-2} and overlay the predicted curves using fixed parameter values of S, k_a, and k_b for different V_E and V_R. The results of these experiments are shown in Fig. 8. The model slightly underpredicts the effect of increasing the anolyte reservoir volume, and largely misses the effect of changing the electrolyzer volume. The data gathered with V_E = 0.0036 L was obtained by assembling the electrolyzer using a thinner PMMA plate for the anode chamber, altering the cell geometry and bringing the anode closer to the separator. Eq. (9) predicts that changing V_E while keeping V_A constant should have no change on the accumulated H_2O_2 concentration. However, it appears that modeling the anodic oxidation of H_2O_2 as a surface reaction using a homogeneous concentration value across the electrolyzer chamber was insufficient to model the system. It is likely that the effect of cell geometry is too significant to be captured by a first order expression using a homogeneous concentration. Future refinement of this model should instead use a mass transfer expression based on electrolyzer geometry to find a surface H_2O_2 concentration value and examine different electrolyzer geometries and current densities to validate the expression.

Table 2
Summary of parameter values from fitted data. Entries marked "(fit)" were fitted using Eq. (9) or (15), while the others were derived from available data. E_{Cell} indicates the full cell potential.

This work	A/cm^2	V_R/L	V_E/L	$\dot{Q}$/L min^{-1}
	10	0.3916	0.0084	0.1
	S/mmol min^{-1} cm^{-2}		k_a (fit)/cm min^{-1}	k_b/min^{-1}
100 mA cm^{-2} (E_{Cell} ~ 5.5 V)		0.017	0.136	1.85 × 10^{-3}
200 mA cm^{-2} (E_{Cell} ~ 7.5 V)		0.037	0.304	1.85 × 10^{-3}
300 mA cm^{-2} (E_{Cell} ~ 9.1 V)		0.054	0.349	1.85 × 10^{-3}
Pangotra et al. [23]	A/cm^2	V_R/L	V_E/L	$\dot{Q}$/L min^{-1}
	10	0.191024	0.008976	0.1
	S (fit)/mmol min^{-1} cm^{-2}		k_a (fit)/cm min^{-1}	k_b/min^{-1}
100 mA cm^{-2} (E_{Cell} ~ 4.4 V)		0.016	0.423	5.7 × 10^{-4}
200 mA cm^{-2} (E_{Cell} ~ 5.9 V)		0.036	0.641	5.7 × 10^{-4}
300 mA cm^{-2} (E_{Cell} ~ 6.7 V)		0.069	1.830	5.7 × 10^{-4}
Li et al. [22]	A/cm^2	V_R/L	V_E/L	$\dot{Q}$/L min^{-1}
	0.5	0	0.06	0
	S/mmol min^{-1} cm^{-2}		k_a (fit)/cm min^{-1}	k_b/min^{-1}
2.3 V vs. RHE (~25 mA cm^{-2})		6.37 × 10^{-3}	0.456	1.83 × 10^{-3}
2.5 V vs. RHE (~42 mA cm^{-2})		8.88 × 10^{-3}	0.707	1.83 × 10^{-3}
2.7 V vs. RHE (~69 mA cm^{-2})		0.013	1.113	1.83 × 10^{-3}

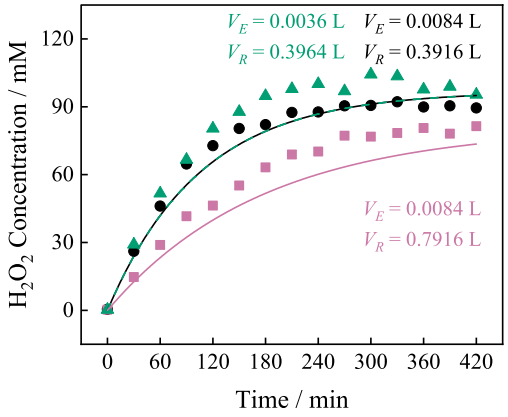

Fig. 8. Experimental validation of the model for different V_E and V_R at 200 mA cm^{-2}. The lines show the predicted concentration curves for the given parameters. The predicted concentrations for the base case (black line) and the lowered V_E case (green line) overlap completely because the total anolyte volume, V_A, was not changed. The prediction for changing V_R underpredicts the experiment, and the prediction for changing V_E does not match.

Because the effect of changing V_R was predicted relatively well, we extend the predictions to other values of V_R, using a base case with V_E = 0.0084 L and V_R = 0.3916 L as per our experimental setup. These predictions are shown in Fig. 9(a). As expected by examination of Eq. (10), decreasing V_R leads to higher steady state concentrations. Fig. 9(a) also shows that decreasing V_R leads to higher concentrations of H_2O_2 earlier in time as the anolyte is charged with H_2O_2. However, due to the large change in anolyte volume with V_R, the trend for the total number of moles is reversed. Fig. 9(b) shows the predicted accumulation of H_2O_2 in moles, where a low V_R achieves a correspondingly low amount

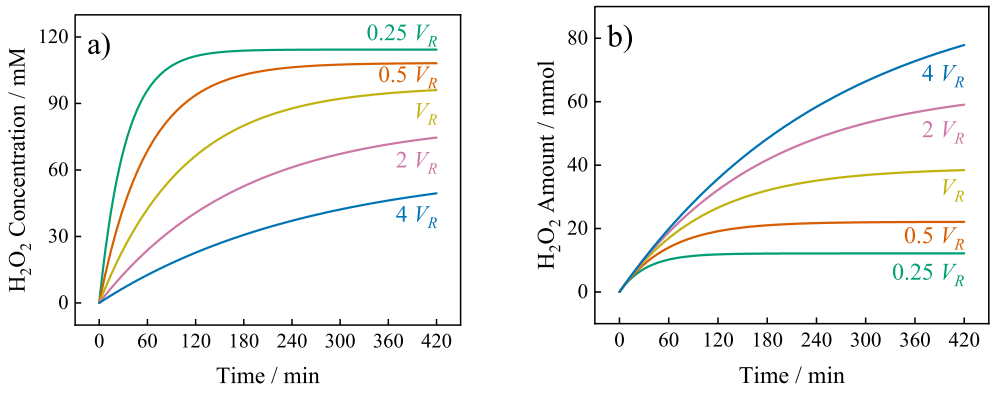

Fig. 9. Simulated results using Eq. (9) at 200 mA cm^{-2} with changing reservoir volume, with V_R = 0.3916 L and V_E = 0.0084 L. (a) The concentration of H_2O_2 reaches a higher steady state value more quickly with decreasing V_R. As V_R approaches 0, the predicted curve approaches the case of a batch reactor. (b) Simulated results for the amount of H_2O_2 in mmol at 200 mA cm^{-2} with changing reservoir volume, V_R. Because the total electrolyte volume decreases strongly with decreasing V_R, the total number of moles produced also decreases.

of H_2O_2, reversing the trend seen in Fig. 9(a). Therefore, the target H_2O_2 production rate must be considered in tandem with the system geometry to find the optimal design parameters and recirculation time. This could be accomplished by setting a desired extent of reaction, ξ, or a desired reaction time, t_ξ, and then optimizing for the number of moles of H_2O_2.

5. Conclusions

The large-scale electrochemical production of H_2O_2 is hampered by low single-pass conversion, and thus requires electrolyte recirculation to charge the anolyte with enough H_2O_2 for further separation. Our work provides an analytical solution for how the concentration develops over time and a methodology to find individual reaction terms for a given system geometry. With simple experimentation, the individual rate constants for anodic generation and bulk disproportionation of H_2O_2 can be quantified. A rate constant for anodic oxidation can then be numerically fitted, but this value is best taken as an estimation of the anodic oxidation for a particular electrolyzer geometry. We found for our system, as well as two others in literature, that the H_2O_2 decomposition due to anodic oxidation was always greater than the decomposition due to bulk disproportionation. As a result of describing anodic oxidation using a homogeneous concentration across the electrolyzer chamber, our analytical model predicted that changing the volume of electrolyte in the anode chamber would have no effect on the achieved concentration of H_2O_2. However, this description was found to be unsuitable for a differing electrolyzer geometry, and the model should be refined with a more generalized expression that accounts for electrolyzer geometry and mass transfer in order to extend the model using surface concentrations. We recommend that the anolyte reservoir volume, V_R, be selected to meet the target production rate at a desired reaction time, but further work can be done to find the optimal balance between these parameters and the overall cost of the scaled-up system.

CRediT authorship contribution statement

Sohan A. Phadke: Conceptualization, Methodology, Investigation, Formal analysis, Writing – original draft, Writing – review & editing. **Wiebren de Jong:** Conceptualization, Writing – review & editing, Supervision, Funding acquisition. **J.W. Haverkort:** Conceptualization, Writing – review & editing, Supervision, Funding acquisition.

Declaration of competing interest

The authors declare that they have no known competing financial interests or personal relationships that could have appeared to influence the work reported in this paper.

Data availability

Data will be made available on request.

Acknowledgments

This project received funding from the NWO-AES Crossover program, Netherlands under project number 17621 (RELEASE). We would like to thank Dr. J. G. Buijnsters for his knowledge and supply of boron-doped diamond electrodes and Mr. Antonius Waskito W. for his assistance with experiments. We would also like to thank Pangotra et al. and Li et al. for making their data readily available.

Appendix A. Low flow rate solution to Eq. (7)

Starting with Eq. (7), we make the following substitutions:

$$\frac{d^2c}{dt^2} + \alpha\frac{dc}{dt} + \beta c = \gamma \tag{A.1}$$

$$\alpha = \frac{\dot{Q}}{V_E} + \frac{\dot{Q}}{V_R} + \frac{k_a A}{V_E} + 2k_b \quad ;$$

$$\beta = \dot{Q}\left(\frac{k_a A}{V_E V_R} + \frac{k_b}{V_R} + \frac{k_b}{V_E}\right) + \frac{k_a A k_b}{V_E} + k_b^2 \quad ; \quad \gamma = \frac{SA\dot{Q}}{V_E V_R}$$

This leads to the general solution,

$$c = C_1\exp\left(-\lambda_1 t\right) + C_2\exp\left(-\lambda_2 t\right) + \frac{\gamma}{\beta} \tag{A.2}$$

where C_1 and C_2 are constants, and

$$\lambda_1 = \frac{\alpha - \sqrt{\alpha^2 - 4\beta}}{2} \quad ; \quad \lambda_2 = \frac{\alpha + \sqrt{\alpha^2 - 4\beta}}{2}$$

Using the initial conditions that $c(t) = 0$ at $t = 0$ and $dc(t)/dt = (SA)/V_R$ at $t = 0$, we arrive at the complete solution in Eq. (A.3).

$$c = \left(\frac{SA\beta - \gamma\lambda_2 V_R}{\beta V_R\left(\lambda_2 - \lambda_1\right)}\right)\exp\left(-\lambda_1 t\right) - \left(\frac{SA\beta - \gamma\lambda_1 V_R}{\beta V_R\left(\lambda_2 - \lambda_1\right)}\right)\exp\left(-\lambda_2 t\right) + \frac{\gamma}{\beta} \tag{A.3}$$

At t approaches ∞, the steady state concentration reached can be expressed as Eq. (A.4),

$$c_{\text{Steady State}} = \frac{\gamma}{\beta} = \frac{SA}{k_a A + k_b\left(V_E + V_R\right) + \frac{k_a A k_b V_R}{\dot{Q}} + \frac{k_b^2 V_E V_R}{\dot{Q}}} \tag{A.4}$$

which simplifies to Eq. (10) for large $\dot{Q}$.

Appendix B. High flow rate justification

In Section 2.4, we use a simplification of Eq. (7) in the case of large $\dot{Q}$. Here, we fix the values of S, A, k_a, k_b, V_E, and V_R using the values for our setup at 200 mA cm^{-2}, and vary $\dot{Q}$ in Eq. (A.3) to confirm that our assumption is valid. Using a base case of $\dot{Q}$ = 0.1 L min^{-1}, as used in our experiments, we show the predicted effect of changing $\dot{Q}$ using Eq. (A.3) in Fig. B.1. The curves for the fastest three flow rates (2 $\dot{Q}$, $\dot{Q}$, and 0.5 $\dot{Q}$) overlap, indicating that our flow rate of $\dot{Q}$ = 0.1 L min^{-1} was sufficiently fast to use Eq. (9) in our analysis.

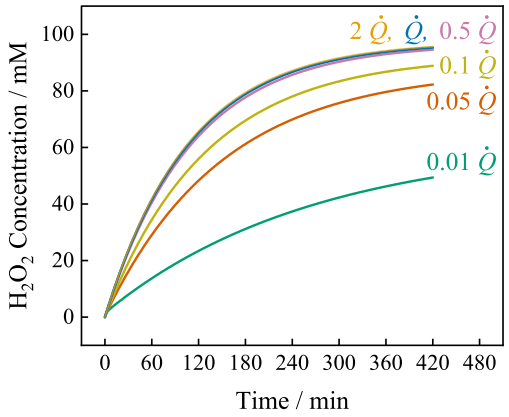

Fig. B.1. Simulated results for changing flow rate, $\dot{Q}$, where the highest three flow rates (corresponding to 0.2, 0.1, and 0.05 L min^{-1}) overlap, indicating the validity of the high flow rate assumption at 0.1 L min^{-1}.

References

[1] P. Bajpai, Biermann's Handbook of Pulp and Paper: Raw Material and Pulp Making, Joseph P. Hayton, Radarweg 29, PO Box 211, 1000 AE Amsterdam, Netherlands, 2018.

[2] J. Ferdush, K. Nahar, T. Akter, M.J. Ferdoush, N. Jahan, S.M.F. Iqbal, Effect of hydrogen peroxide concentration on 100% cotton knit fabric bleaching, Eur. Sci. J. 15 (2019) 254–263, http://dx.doi.org/10.19044/esj.2019.v15n33p254.

[3] Q. Chen, Toward cleaner production of hydrogen peroxide in China, J. Clean. Prod. 14 (2006) 708–712, http://dx.doi.org/10.1016/j.jclepro.2005.03.025.

[4] Q. Chen, Development of an anthraquinone process for the production of hydrogen peroxide in a trickle bed reactor–from bench scale to industrial scale, Chem. Eng. Process.: Process Intensif. 47 (2008) 787–792, http://dx.doi.org/10.1016/j.cep.2006.12.012.

[5] A.T. Murray, S. Voskian, M. Schreier, T.A. Hatton, Y. Surendranath, Electrosynthesis of hydrogen peroxide by phase-transfer catalysis, Joule 3 (2019) 2942–2954, http://dx.doi.org/10.1016/j.joule.2019.09.019.

[6] A.J. Shih, M.C.O. Monteiro, F. Datilla, D. Pavesi, M. Philips, A.H.M. da Silva, R.E. Vos, K. Ojha, S. Park, O. van der Heijden, G. Marcandalli, A. Goyal, M. Villalba, X. Chen, G.T.K.K. Gunasooriya, I. McCrum, R. Mom, N. López, M.T.M. Koper, Water electrolysis, Nature Rev. Methods Prim. 2 (2022) 1–19, http://dx.doi.org/10.1038/s43586-022-00164-0.

[7] C. Qu, D.-w. Liang, Novel electrochemical advanced oxidation processes with H_2O_2 generation cathode for water treatment: A review, J. Environ. Chem. Eng. 10 (2022) 107896, http://dx.doi.org/10.1016/j.jece.2022.107896.

[8] V. Viswanathan, H.A. Hansen, J.K. Nørskov, Selective electrochemical generation of hydrogen peroxide from water oxidation, J. Phys. Chem. Lett. 6 (2015) 4224–4228, http://dx.doi.org/10.1021/acs.jpclett.5b02178.

[9] S. Mavrikis, S.C. Perry, P.K. Leung, L. Wang, C. Ponce de León, Recent advances in electrochemical water oxidation to produce hydrogen peroxide: A mechanistic perspective, ACS Sustain. Chem. Eng. 9 (2021) 76–91, http://dx.doi.org/10.1021/acssuschemeng.0c07263.

[10] T.M. Gill, L. Vallez, X. Zheng, The role of bicarbonate-based electrolytes in H_2O_2 production through two-electron water oxidation, ACS Energy Lett. 6 (2021) 2854–2862, http://dx.doi.org/10.1021/acsenergylett.1c01264.

[11] S. Siahrostami, G.-L. Li, V. Viswanathan, J.K. Nørskov, One- or two-electron water oxidation, hydroxyl radical, or H_2O_2 evolution, J. Phys. Chem. Lett. 8 (2017) 1157–1160, http://dx.doi.org/10.1021/acs.jpclett.6b02924.

[12] X. Shi, S. Siahrostami, G.-L. Li, Y. Zhang, P. Chakthranont, F. Studt, T.F. Jaramillo, X. Zheng, J.K. Nørskov, Understanding activity trends in electrochemical water oxidation to form hydrogen peroxide, Nature Commun. 8 (2017) 1–12, http://dx.doi.org/10.1038/s41467-017-00585-6.

[13] A. Venugopal, L.H.T. Egberts, J. Meeprasert, E.A. Pidko, B. Dam, T. Burdyny, V. Sinha, W.A. Smith, Polymer modification of surface electronic properties of electrocatalysts, ACS Energy Lett. 7 (2022) 1586–1593, http://dx.doi.org/10.1021/acsenergylett.2c00199.

[14] K. Fuku, Y. Miyase, Y. Miseki, T. Gunji, K. Sayama, Enhanced oxidative hydrogen peroxide production on conducting glass anodes modified with metal oxides, Chem. Select 1 (2016) 5721–5726, http://dx.doi.org/10.1002/slct.201601469.

[15] Y. Miyase, S. Iguchi, Y. Miseki, T. Gunji, K. Sayama, Electrochemical H_2O_2 production and accumulation from H_2O by composite effect of Al_2O_3 and $BiVO_4$, J. Electrochem. Soc. 166 (2019) H644–H649, http://dx.doi.org/10.1149/2.0561913jes.

[16] T. Kang, B. Li, Q. Hao, W. Gao, F. Bin, K.N. Hui, D. Fu, B. Dou, Efficient hydrogen peroxide (H_2O_2) synthesis by $CaSnO_3$ via two-electron water oxidation reaction, ACS Sustain. Chem. Eng. 8 (2020) 15005–15012, http://dx.doi.org/10.1021/acssuschemeng.0c05449.

[17] S. Mavrikis, M. Göltz, S.C. Perry, F. Bogdan, P.K. Leung, S. Rosiwal, L. Wang, C. Ponce de León, Effective hydrogen peroxide production from electrochemical water oxidation, ACS Energy Lett. 6 (2021) 2369–2377, http://dx.doi.org/10.1021/acsenergylett.1c00904.

[18] C. Xia, S. Back, S. Ringe, K. Jiang, F. Chen, X. Sun, S. Siahrostami, K. Chan, H. Wang, Confined local oxygen gas promotes electrochemical water oxidation to hydrogen peroxide, Nat. Catal. 3 (2020) 125–134, http://dx.doi.org/10.1038/s41929-019-0402-8.

[19] D. Pickett, The analysis of a batch electrochemical reactor with continuously recirculating electrolyte, Electrochim. Acta 18 (1973) 835–837, http://dx.doi.org/10.1016/0013-4686(73)85035-2.

[20] T.M. Gill, X. Zheng, Comparing methods for quantifying electrochemically accumulated H_2O_2, Chem. Mater. 32 (2020) 6285–6294, http://dx.doi.org/10.1021/acs.chemmater.0c02010.

[21] H.H.B. Lee, A.-H. Park, C. Oloman, Stability of hydrogen peroxide in sodium carbonate solutions, Tappi J. 83 (2000) 1–9.

[22] L. Li, Z. Hu, Y. Kang, S. Cao, L. Xu, L. Yu, L. Zhang, J.C. Yu, Electrochemical generation of hydrogen peroxide from a zinc gallium oxide anode with dual active sites, Nature Commun. 14 (2023) 1–12, http://dx.doi.org/10.1038/s41467-023-37007-9.

[23] D. Pangotra, L.-I. Csepei, A. Roth, V. Sieber, L. Vieira, Anodic generation of hydrogen peroxide in continuous flow, Green Chem. 24 (2022) 7931–7940, http://dx.doi.org/10.1039/d2gc02575b.